XLVI CILAMCE
VITÓRIA - ES - BRAZIL - 2025
XLVI IBERO-LATIN AMERICAN CONGRESS ON COMPUTATIONAL METHODS IN ENGENEERING

Machine-precision implementation of higher-order, generally curved boundary elements for three-dimensional problems

Ney Augusto Dumont[1]

[1]*Dept. of Civil and Environmental Engineering, Pontifical Catholic University of Rio de Janeiro*
Rua Marquês de São Vicente 225, 22451900, Rio de Janeiro, Brazil

Abstract. The author recently revisited the collocation boundary element method for its consistency. Arbitrary rigid-body displacements, as for elasticity of a finite domain, are naturally taken into account, and traction force parameters are always in balance independently of problem scale and mesh discretization. For generally curved boundaries, the correct definition of traction force interpolation functions enables the enunciation of a general convergence theorem, the introduction of patch and cut-out tests for precision and accuracy assessments, and, most importantly, a considerable simplification of the numerical implementations. The formulation became extremely simple to code for two-dimensional elasticity problems in terms of a complex variable, with precision only limited by the machine and less liable to round-off errors than its real-variable counterpart: precision is only conditioned by the Gauss-Legendre quadrature of the regular parts of the integrands. We now present the three-dimensional version of such general implementation for potential and elasticity problems, which is only apparently less intuitive, since it is based on the same concepts of a complex quasi-singularity. A more general mathematical framework is required, which resorts to the hypercomplex – but surprisingly simple – description of the problem's geometry, as we have been able to develop. The old concepts of geometric near singularities – with many badly and highly constrained approximating solutions – should be abandoned in the face of the proposed general, precise, and accurate methodology. We present the basics of this new formulation, which applies to all kinds and degrees of singularities and any topologically challenging problems. The complete formulation will be published in an extended paper.

Keywords: Consistent boundary elements, Collocation, Isoparametric analysis, Three-dimensional problems, High-order elements

1 Introduction

Our recent proposition of the "consistent" collocation boundary element method (CBEM) has required a long maturation time since the first attempt of over 30 years ago [1]. Some contributions followed sparsely [2–4] until the three-paper publication [5–7], which brought the theoretical basis for general linear problems of steady-state potential and elastostatics, with code-implementation and applications for the two-dimensional (2D) case. A fully complex-variable reformulation followed quite recently [8], with friendlier equations and code implementation.

Despite the sound mathematics laid down in these papers, the question "can we do better?" (for the particular case of 2D linear problems of elastostatics and steady-state potential) persisted concerning the efficient numerical simulation in terms of eventually optimal node location inside a boundary element, efficient, homothetic mesh-refinement, and accurate geometry representation. This is in our latest paper, published in memory of our loved Patrick Selvadurai [9]. We show that the denomination "geometry-preserving" is more informative than and not committed to the term "isogeometric" proposed by Hughes [10] for widespread applications also in the frame of the boundary element method – which did not take into account the mathematical consistency of our developments.

Paper [9], with title "Consistent Boundary Element Method for Two-Dimensional Problems of Elasticity with Geometry-Preserving, Homothetic Element Generation", can be arguably considered the *nec plus ultra*, the ultimate contribution to the boundary-element analysis of two-dimensional elastostatics.

But here comes the inevitable question: What about three-dimensional problems?

We can now proudly announce that the 3D problem has been solved! The corresponding developments – including accurate evaluations for topologically challenging problems – are about to be published in a special issue of EABE dedicated to José Dominguez, a pioneer in the field of boundary elements who left us recently.

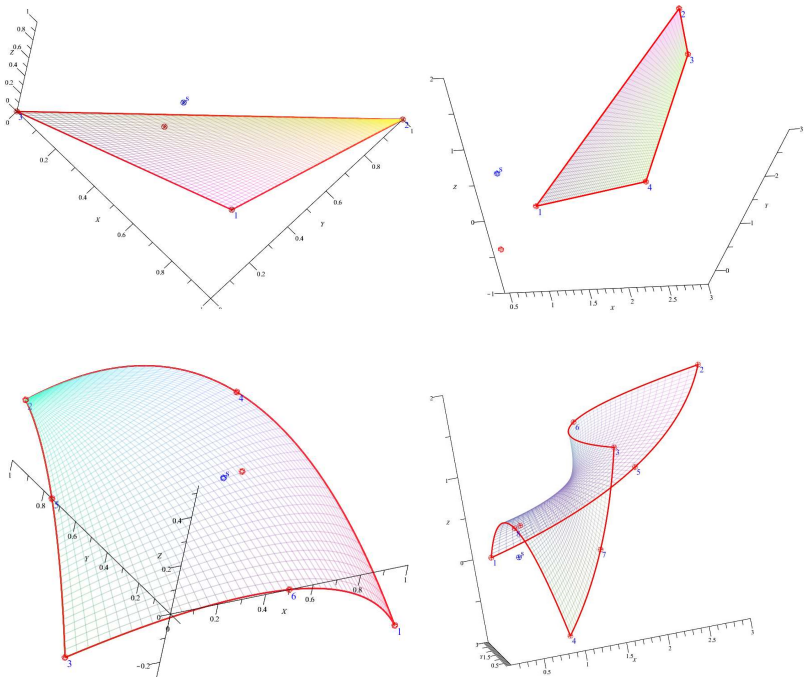


Figure 1. Plots of elements T3, Q4, T6 and Q8 of nodal coordinates given in Table 1. A blue dot "s" indicates a source point of global coordinates $\mathbf{x}_s = (0.44, 0.4, 0.22)$, the red dot is its projection onto the element's surface.

The present contribution outlines just the basics of our latest achievements: the correct representation of the source point in complex natural coordinates and the evaluation of generally singular or quasi-singular integrals.

2 From Cartesian hypercomplex into natural complex coordinates of a source point

The reader is strongly recommended to consult [5] and then have an overview of [9, 11]. It is mentioned in Footnote [20] of [11] that the term "complex" in the title of [1] may have been "bad marketing" (since readers might mistakenly argument that their problem's equations are in real variables), with the complement "(h)owever, it could not be more precise mathematically". The BEM developers resorted to the qualification "near" for integrals related to small distances from source to field points. We emphatically proposed from the beginning [1] to use the word "quasi",[1] and here also emphatically refer the reader to at least the introductory part of [9].

A boundary segment (or *boundary element*) of the three-dimensional (3D) body is defined as Γ_{seg} in terms of natural coordinates (ξ, η) with local support. These natural coordinates span

$$\begin{aligned} &\xi \in [0, 1-\eta], \qquad \eta \in [0, 1], \quad \text{for triangle elements} \\ &\xi \in [-1, 1], \qquad \eta \in [-1, 1], \quad \text{for quadrilateral elements} \end{aligned} \tag{1}$$

for the description of generally distorted elements, such as illustrated in Fig. 1 according to the nodal data of Table 1 in reference to Fig. 2. This isoparametric description of both mechanical quantities and geometry along a boundary segment Γ_{seg} is inherited from the finite element method (FEM): an improvement is proposed in [9].

We introduce the hypercomplex coordinate notation for the 3D Cartesian coordinates $\mathbf{x} \equiv (x, y, z)$:

$$\zeta = \zeta_0 + ix + jy + kz \ \in \mathbb{H} \tag{2}$$

where $\mathbb{H}$ stands for *hypercomplex* or *quaternion*[2]. The hyper-imaginary parts of a hypercomplex number are

[1] From Merriam-Webster dictionary, "near" means "at, within, or to a short distance or time", and "quasi" stands for "having some resemblance usually by possession of certain attributes". We exemplify with the terms "quasi-static" and "quasi-stellar", where "near" would be completely inappropriate, as well as presently (Footnote 9 of [9]). Observe that "quasi" could not figure in the expression "near-earth orbiting satellite". When a source point is close to, or near a boundary segment, the corresponding integral is quasi-singular, not nearly singular.

[2] See, for instance, https://mathworld.wolfram.com/HypercomplexNumber.html.

represented by "i", "j" and "k", whose mutual multiplication is non-commutative :

$$\begin{array}{lll} ij = k & ji = -k & ii = -1 \\ jk = i & kj = -i & jj = -1 \\ ki = j & ik = -j & kk = -1 \end{array} \tag{3}$$

The vector of hypercomplex nodal coordinates of a boundary segment is defined as

$$\mathbf{C} = \left\langle ix_1 + jy_1 + kz_1 \quad ix_2 + jy_2 + kz_2 \quad \ldots \quad ix_{n_{en}} + jy_{n_{en}} + kz_{n_{en}} \right\rangle \quad \in \mathbb{H} \tag{4}$$

whose dimension – number of element nodes n_{en} – is either 3, 4, 6 or 8, referring to the T3, Q4, T6 or Q8 element, as presently implemented, and with coordinates initially referred to the origin of the Cartesian system. We subsequently refer these coordinates to the source point s considered in the specific step of the code implementation.

The local, natural coordinates referred to a given boundary segment are generalized as the complex

$$(\xi, \eta) = (a + ic, b + id) \quad \in \mathbb{C} \tag{5}$$

where a, b are the real parts, and the imaginary parts $c \neq 0, d \neq 0$ denote that the point is outside not only Γ_{seg} but also its extension described by the real coordinates (ξ, η), as to be eventually required.

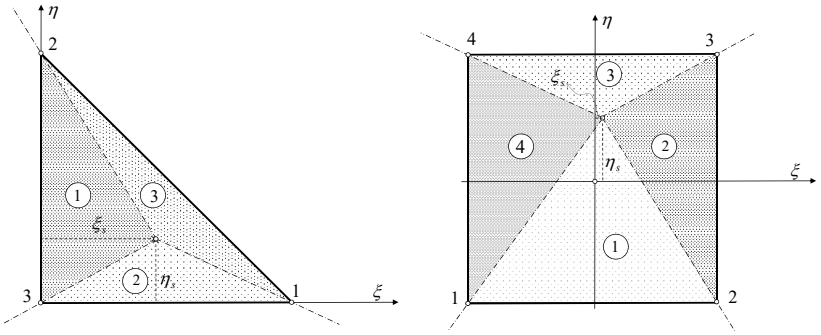


Figure 2. Reference triangle and square elements with natural coordinates (ξ, η) in the frame of an isoparametric description. Generically complex subtriangles have as common vertex the complex source point (ξ_s, η_s).

Table 1. Nodal coordinates of the triangle and quadrilateral elements of Fig. 1, and evaluated complex coordinates (ξ_s, η_s) for the source point $\mathbf{x}_s = (0.44, 0.4, 0.22)$. The closest points (ξ_d, η_d) are shown just for curiosity.

Element type	Nodal coordinates	Source points $\langle \xi_s, \eta_s \rangle^{\mathrm{T}}$	$\langle \xi_d, \eta_d \rangle^{\mathrm{T}}$
T3	$\begin{bmatrix} 1 & 1 & 0 \\ 0 & 1 & 0 \\ 1 & 0 & 0 \end{bmatrix}$	$\begin{Bmatrix} 0.13 + 0.09i \\ 0.31 - 0.09i \end{Bmatrix}$	$\begin{Bmatrix} 0.16 \\ 0.34 \end{Bmatrix}$
Q4	$\begin{bmatrix} 1 & 3 & 2 & 1.5 \\ 0 & 1 & 3 & 2 \\ 0 & 2 & 0.1 & -1 \end{bmatrix}$	$\begin{Bmatrix} -1.4233 + 0.33666i \\ -1.0730 - 0.84619i \end{Bmatrix}$	$\begin{Bmatrix} -1.0718 \\ -0.87831 \end{Bmatrix}$
T6	$\begin{bmatrix} 1 & 0 & 0 & 0.5 & 0 & 0.5 \\ 0 & 1 & 0.5 & 0.5 & 0.75 & 0 \\ -0.25 & 0.25 & -0.5 & 0.5 & 0 & 0 \end{bmatrix}$	$\begin{Bmatrix} 0.44 \\ 0.29413 + 0.094072i \end{Bmatrix}$	$\begin{Bmatrix} 0.37793 \\ 0.29938 \end{Bmatrix}$
Q8	$\begin{bmatrix} 0.1 & 3 & 2 & 1 & 2 & 1.5 & 1.5 & 0.5 \\ 0.2 & 1 & 3 & 2 & 0.5 & 2 & 1.5 & 1 \\ 0.3 & 2 & 1 & -1 & 1 & 1.5 & 0 & 0.5 \end{bmatrix}$	$\begin{Bmatrix} -0.92822 - 0.25068i \\ 0.001675 + 0.52928i \end{Bmatrix}$	$\begin{Bmatrix} -0.85323 \\ -1.0505 \end{Bmatrix}$

As illustrated in Figs. 1, 2 and Table 1, Lagrangian and Serendipity incomplete polynomials (ξ, η) of any order for generally curved quadrilaterals, and complete polynomials (ξ, η) for curved triangular boundary segments, are primarily required for the accurate numerical implementation of the BEM for 3D potential problems. These functions are inherited from the FEM [12] and are here collectively denoted *interpolation polynomials*.

The same interpolation polynomials used for the approximate interpolation of mechanical quantities along a boundary segment Γ_{seg} are used for the geometry, in the frame of an *isoparametric formulation*:

$$\mathbf{N}^{\mathrm{T}}(\xi,\eta)=\begin{bmatrix}N_1(\xi,\eta) & \dots & N_{n_{en}}(\xi,\eta)\end{bmatrix} \quad \in \mathbb{R} \tag{6}$$

The interpolation polynomials $N_m(\xi,\eta)$ are conceived to refer to points only on the boundary segment Γ_{seg} to which they are assigned, mathematically speaking with *local support*, as in the FEM. However, an extension of this concept is necessary for dealing with quasi-singularity issues. This follows the same pattern of the 2D formulation [5]. Then, the exact mathematical implementation will eventually require evaluations such that $\mathbf{N}(\xi,\eta)\in\mathbb{C}$.

2.1 From hypercomplex global $\zeta_s = ix_s + jy_s + kz_s$ into complex natural coordinates $(a_s + ic_s, b_s + id_s)$

We describe the hypercomplex coordinates $\mathbf{x}_s \equiv (x_s, y_s, z_s)$ of a source point s, according to Eq. (2), in terms of complex natural coordinates (ξ_s, η_s) referred to a boundary segment Γ_{seg} as

$$\zeta_s = ix_s + jy_s + kz_s = \mathbf{CN}(\xi_s,\eta_s) \equiv \mathbf{CN}(a_s + ic_s, b_s + id_s) \quad \in \mathbb{H} \tag{7}$$

This may be expanded, observing Eq. (3), as

$$\begin{aligned}
&\mathbf{CN}(a_s{+}ic_s,b_s{+}id_s) = (i\mathbf{C}_x{+}j\mathbf{C}_y{+}k\mathbf{C}_z)\,(\Re(\mathbf{N}(a_s{+}ic_s,b_s{+}id_s)){+}i\Im(\mathbf{N}(a_s{+}ic_s,b_s{+}id_s)))\\
&=(i\mathbf{C}_x{+}j\mathbf{C}_y{+}k\mathbf{C}_z)\,\Re(\mathbf{N}(a_s{+}ic_s,b_s{+}id_s)){+}(-\mathbf{C}_x{+}j\mathbf{C}_z-k\mathbf{C}_y)\,\Im(\mathbf{N}(a_s{+}ic_s,b_s{+}id_s))\\
&\equiv[-\mathbf{C}_x\mathbf{N}_\Im{+}i\mathbf{C}_x\mathbf{N}_\Re{+}j(\mathbf{C}_y\mathbf{N}_\Re{+}\mathbf{C}_z\mathbf{N}_\Im){+}k(\mathbf{C}_z\mathbf{N}_\Re-\mathbf{C}_y\mathbf{N}_\Im)]_s
\end{aligned} \tag{8}$$

where the real and imaginary parts of $\mathbf{N}(a_s + ic_s, b_s + id_s) = \Re(\mathbf{N}) + i\Im(\mathbf{N})$ are pre-evaluated analytically (and stored, for general code implementation). This leads to a system of four equations, counting the real part and the three hyper-imaginary parts $(\Im_i, \Im_j, \Im_k)$, also with four unknowns, namely, (a_s, c_s, b_s, d_s):

$$\left\{\begin{array}{l}
\Re(\mathbf{CN}(a_s,c_s,b_s,d_s)) = 0\\
\Im_i(\mathbf{CN}(a_s,c_s,b_s,d_s)) = x_s\\
\Im_j(\mathbf{CN}(a_s,c_s,b_s,d_s)) = y_s\\
\Im_k(\mathbf{CN}(a_s,c_s,b_s,d_s)) = z_s
\end{array}\right\} \tag{9}$$

Except for the T3 triangle and the flat Q4 quadrilateral elements, the system matrix of Eq. (9) is not constant. The immediate possibility of solving this system is in terms of Newton-Raphson iterations:

$$\begin{Bmatrix}a_s\\b_s\\c_s\\d_s\end{Bmatrix}_{(l+1)} = \begin{Bmatrix}a_s\\b_s\\c_s\\d_s\end{Bmatrix}_{(l)} + \begin{bmatrix}
\dfrac{\partial\Re(\mathbf{CN})}{\partial a} & \dfrac{\partial\Re(\mathbf{CN})}{\partial b} & \dfrac{\partial\Re(\mathbf{CN})}{\partial c} & \dfrac{\partial\Re(\mathbf{CN})}{\partial d}\\
\dfrac{\partial\Im_i(\mathbf{CN})}{\partial a} & \dfrac{\partial\Im_i(\mathbf{CN})}{\partial b} & \dfrac{\partial\Im_i(\mathbf{CN})}{\partial c} & \dfrac{\partial\Im_i(\mathbf{CN})}{\partial d}\\
\dfrac{\partial\Im_j(\mathbf{CN})}{\partial a} & \dfrac{\partial\Im_j(\mathbf{CN})}{\partial b} & \dfrac{\partial\Im_j(\mathbf{CN})}{\partial c} & \dfrac{\partial\Im_j(\mathbf{CN})}{\partial d}\\
\dfrac{\partial\Im_k(\mathbf{CN})}{\partial a} & \dfrac{\partial\Im_k(\mathbf{CN})}{\partial b} & \dfrac{\partial\Im_k(\mathbf{CN})}{\partial c} & \dfrac{\partial\Im_k(\mathbf{CN})}{\partial d}
\end{bmatrix}^{-1}_{(l)} \begin{Bmatrix}-\Re(\mathbf{CN})\\x_s-\Im_i(\mathbf{CN})\\y_s-\Im_j(\mathbf{CN})\\z_s-\Im_k(\mathbf{CN})\end{Bmatrix}_{(l)} \tag{10}$$

where $(l+1)$ denotes an improved value obtained from some initial approximate result (l).

Table 1 presents in the second column the nodal coordinates of the elements illustrated in Fig. 1. The second column shows the results from Eq. (10), which are to compare with the mere (presently useless) projections of the source points onto the elements' surfaces, in the fourth column.

We can never overstate that rather than Cartesian geometry the important fact is how the source point is described in terms of the natural coordinates primarily referred to a boundary segment's surface.

3 Machine-precision evaluation of singularities and quasi-singularities for 3D problems

Let $f(\xi-\xi_s,\eta-\eta_s)\equiv f(\Delta\xi,\Delta\eta)$ be a regular function[3]. The singularity of a boundary element integral is related to the eventuality of a relatively small term $\left(\Delta\xi^2+\Delta\eta^2\right)^{m/2}$ in the denominator, where

$$\begin{aligned} &m=0 \quad \Rightarrow \text{no singularity}\\ &m=1 \quad \Rightarrow \text{“weak” singularity or quasi-singularity as for the single-layer potential matrix } \mathbf{G}\\ &m=3 \quad \Rightarrow \text{singularity or quasi-singularity as for the double-layer potential matrix } \mathbf{H}\\ &m=5 \quad \Rightarrow \text{strong quasi-singularity as in part of the expression of gradient or stress results} \end{aligned} \tag{11}$$

Independently of the value of m, integration of $f(\Delta\xi,\Delta\eta)/\left(\Delta\xi^2+\Delta\eta^2\right)^{m/2}$ over a subtriangle of Γ_{seg} may be developed in terms of the local coordinate system $(\bar{\bar{\xi}},\bar{\bar{\eta}})$ of Fig. 3 and with reference to Table 2 as[4]

$$\begin{aligned} &\int_0^{\bar{\bar{\eta}}_1}\left(\int_{\bar{\bar{\xi}}_0}^{\bar{\bar{\xi}}_1}\frac{f\left(\Delta\xi,\Delta\eta\right)\mathrm{d}\bar{\bar{\xi}}}{\left(\Delta\xi^2+\Delta\eta^2\right)^{m/2}}\right)\mathrm{d}\bar{\bar{\eta}}=\int_0^{\bar{\bar{\eta}}_1}\left(\int_{\bar{\bar{\xi}}_0}^{\bar{\bar{\xi}}_1}\frac{f\left(\Delta\xi,\Delta\eta\right)}{\left(\bar{\bar{\xi}}^2+\bar{\bar{\eta}}^2\right)^{m/2}}\mathrm{d}\bar{\bar{\xi}}\right)\mathrm{d}\bar{\bar{\eta}}\\ \equiv&\int_0^{\bar{\bar{\eta}}_1}\frac{1}{\bar{\bar{\eta}}^{m-1}}\left(\bar{\bar{\eta}}^{m-1}\int_{\bar{\bar{\xi}}_0}^{\bar{\bar{\xi}}_1}\frac{f\left(\Delta\xi,\Delta\eta\right)}{\left(\bar{\bar{\xi}}^2+\bar{\bar{\eta}}^2\right)^{m/2}}\mathrm{d}\bar{\bar{\xi}}\right)\mathrm{d}\bar{\bar{\eta}}\\ \equiv&f\!\!\!\!\!\!\int_0^{\bar{\bar{\eta}}_1}\frac{1}{\bar{\bar{\eta}}^{m-1}}\left(\int_{\tilde{\bar{\xi}}_0}^{\tilde{\bar{\xi}}_1}\frac{f\left(\Delta\xi,\Delta\eta\right)\mathrm{d}\tilde{\bar{\xi}}}{\left(\tilde{\bar{\xi}}^2+1\right)^{m/2}}\right)\mathrm{d}\bar{\bar{\eta}}\quad\begin{pmatrix}+\text{ eventual local}\\ \text{correction at }\bar{\bar{\eta}}\to 0\end{pmatrix} \end{aligned} \tag{12}$$

The expression in the latter row comes from the further substitution $\bar{\bar{\xi}}\leftarrow\sqrt{\bar{\bar{\eta}}^2}\tilde{\bar{\xi}}$, such that, according to Fig. 3,

$$\int_{\bar{\bar{\xi}}_0}^{\bar{\bar{\xi}}_1}\frac{f\left(\Delta\xi,\Delta\eta\right)\mathrm{d}\bar{\bar{\xi}}}{\left(\bar{\bar{\xi}}^2+\bar{\bar{\eta}}^2\right)^{m/2}}=\int_{\tilde{\bar{\xi}}_0}^{\tilde{\bar{\xi}}_1}\frac{f\left(\Delta\xi,\Delta\eta\right)\sqrt{\bar{\bar{\eta}}^2}\mathrm{d}\tilde{\bar{\xi}}}{\left(\bar{\bar{\eta}}^2\right)^{m/2}\left(\tilde{\bar{\xi}}^2+1\right)^{m/2}}=\bar{\bar{\eta}}^{1-m}\int_{\tilde{\bar{\xi}}_0}^{\tilde{\bar{\xi}}_1}\frac{f\left(\Delta\xi,\Delta\eta\right)\mathrm{d}\tilde{\bar{\xi}}}{\left(\tilde{\bar{\xi}}^2+1\right)^{m/2}} \tag{13}$$

where $(\bar{\bar{\eta}}^2)^{\frac{1-m}{2}}\equiv\bar{\bar{\eta}}^{1-m}$ for m = 1, 3 or 5, thus an odd number. We must give due attention to the correct expression of the evaluation interval for a general complex $\bar{\bar{\eta}}$, as indicated[5]. The evaluation of this integral involves multivalued functions such as $\sinh^{-1}(\tilde{\bar{\xi}})\equiv\ln\left(\tilde{\bar{\xi}}+\sqrt{\tilde{\bar{\xi}}^2+1}\right)$: $\sinh(\tilde{\bar{\xi}})=\sinh(\tilde{\bar{\xi}}+2\,n\,i\,\pi)$, for n an arbitrary integer. However, the integration interval always comprises an angle smaller than 180°, since we are dealing with the internal angles of subtriangles.

These developments hold for all subtriangles of Fig. 3 if we just replace the integration limits and arguments of $f(\Delta\xi,\Delta\eta)$ with the corresponding expressions of Table 2.

In the case of a $1/r$ singularity, as for the matrix **G**, we have $m=1$, which results in a regular integral in both variables $\bar{\bar{\xi}}$ and $\bar{\bar{\eta}}$. In such case, Gauss-Legendre quadrature may be successively applied to the integrals after interval normalization. If $m=3$ or $m=5$, as required either in the evaluation of matrix **H** or in part expressing stress or gradient values in the domain, the integral in $\bar{\bar{\eta}}$ is to be evaluated in terms of finite parts, which applies trivially to $m=1$. If $m=3$ and we are dealing with an actual singularity – for the diagonal terms of **H** –, a discontinuous term must be locally evaluated and added, as indicated (and dealt with in the extended paper).

4 Conclusions

Figure 1 is illustrative of how a source point in 3D Cartesian coordinates (x_s,y_s,z_s) is to be mapped onto the natural coordinates (ξ_s,η_s) of a curved surface Γ_{seg}: by simply resorting to hypercomplex notation. Our proposition of over 30 years ago [1] for 2D problems – represent (x_s,y_s) in terms of a complex ξ_s – still seems (willing or unwilling) strange to a large part of the mathematics and engineering community (who would have to

[3] A function is regular if and only if a polynomial of moderate order can approximate it within an acceptable error tolerance throughout a boundary segment. (“Moderate order” and “acceptable error” depend on the desired precision of an engineering application.)

[4] After half a dozen different attempts including the famous – or infamous – Cartesian-to-polar coordinates transformation.

[5] We prefer to work with the explicit expressions $\bar{\bar{\eta}}/\sqrt{\bar{\bar{\eta}}^2}$ and $\sqrt{\bar{\bar{\eta}}^2}$ above rather than resorting to some coding-dependent *sign* functions.

give up over half a century of misconceptions). The present developments for 3D problems look like a daring step, as hypercomplex numbers must be resorted to, Section 2, but are actually quite natural in the realm of mathematics. Once the generally complex (ξ_s, η_s) is found, according to Eqs. (9) and (10), the rest is plain code implementation.

Equation (12) is too general but adequate – given this paper's space restriction – to show that all types of singularities or quasi-singularities listed in Eq. (11) may be dealt with in principle in a single framework. It makes here more evident that the correct usage is "singularities and quasi-singularities" – no matter the language. (The English "nearly singular" and "near-singularity" are technically wrong constructions – see Footnote 1 – with misleading consequences.) Of course, if the source point is sufficiently far from Γ_{seg} (far versus close are application- and precision-dependent), we just use Dunavant's [13] or Gauss-Legendre quadrature for a whole reference triangle or square, Fig. 2. Otherwise, the indicated subtriangle "division" (for the generically complex common vertex $(\xi_s, \eta_s) \notin \Gamma_{seg}$) is mandatory and Eq. (12) must be resorted to. Two weighted-quadrature procedures – for separate evaluations along $\tilde{\bar{\xi}} \in \left[\tilde{\bar{\xi}}_0, \tilde{\bar{\xi}}_1\right]$ and $\bar{\bar{\eta}} \in (0, \bar{\bar{\eta}}_1]$ have been implemented and tested. Their application is code-intensive but restricted to small source-to-field distances and with precision errors completely under control. An improper integral, for $m = 1$, may be dealt with separately, in a simplified way but including more code lines. The most noticeable fact about the proposed subtriangle implementation is that only linear transformations $(\xi, \eta) \rightarrow \left(\bar{\bar{\xi}}, \bar{\bar{\eta}}\right)$ are involved, then with no introduction of further nonlinearities. This is numerically assessed in the extended paper. Let us close with the advice: never ever use Cartesian to polar transformation!

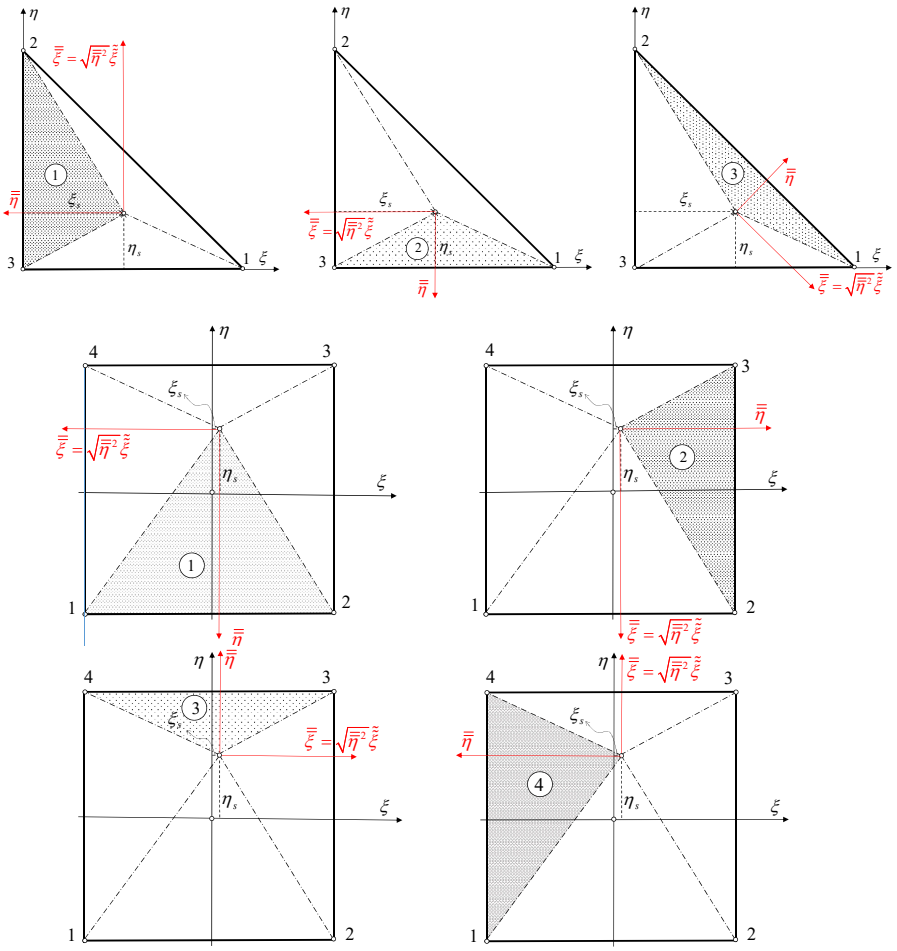


Figure 3. Reference triangle and square of Fig. 2 with natural (ξ, η) transformed into subtriangle coordinates $(\bar{\bar{\xi}}_s, \bar{\bar{\eta}}_s)$. The coordinate $\bar{\bar{\xi}}_s$ is further transformed into $\tilde{\bar{\xi}}_s$. Transformation data are summarized in Table 2.

Acknowledgements. This project was supported by the Brazilian federal agencies CAPES and CNPq, as well as by the state agency FAPERJ.

Authorship statement. The author hereby confirms that he is the sole liable person responsible for the authorship of this work; all material herein included is the property (and authorship) of the author.

Table 2. Basic data for the integration of a function $f(\Delta\xi, \Delta\eta)/r^m$ over subtriangles of either triangle $\triangle$ or quadrilateral $\square$ elements, with natural (ξ, η) transformed into local coordinates $(\tilde{\bar{\xi}}, \bar{\bar{\eta}})$, according to Fig. 3.

	Subtriangles	$\tilde{\bar{\xi}} \in [\tilde{\bar{\xi}}_0, \tilde{\bar{\xi}}_1]$	$\bar{\bar{\eta}} \in (\bar{\bar{\eta}}_0, \bar{\bar{\eta}}_1]$	Arguments of $f(\Delta\xi, \Delta\eta)$
$\triangle$	① $\xi_s \neq 0$	$\left[-\frac{\eta_s}{\xi_s}\frac{\bar{\bar{\eta}}}{\sqrt{\bar{\bar{\eta}}^2}}, \frac{1-\eta_s}{\xi_s}\frac{\bar{\bar{\eta}}}{\sqrt{\bar{\bar{\eta}}^2}}\right]$	$(0, \xi_s]$	$\left(-\bar{\bar{\eta}}, \sqrt{\bar{\bar{\eta}}^2}\tilde{\bar{\xi}}\right)$
	② $\eta_s \neq 0$	$\left[\frac{\xi_s-1}{\eta_s}\frac{\bar{\bar{\eta}}}{\sqrt{\bar{\bar{\eta}}^2}}, \frac{\xi_s}{\eta_s}\frac{\bar{\bar{\eta}}}{\sqrt{\bar{\bar{\eta}}^2}}\right]$	$(0, \eta_s]$	$\left(-\sqrt{\bar{\bar{\eta}}^2}\tilde{\bar{\xi}}, -\bar{\bar{\eta}}\right)$
	③ $1-\xi_s-\eta_s \neq 0$	$\left[\frac{-1-\xi_s+\eta_s}{1-\xi_s-\eta_s}\frac{\bar{\bar{\eta}}}{\sqrt{\bar{\bar{\eta}}^2}}, \frac{1-\xi_s+\eta_s}{1-\xi_s-\eta_s}\frac{\bar{\bar{\eta}}}{\sqrt{\bar{\bar{\eta}}^2}}\right]$	$\left(0, \frac{1-\xi_s-\eta_s}{\sqrt{2}}\right]$	$\left(\frac{\bar{\bar{\eta}}+\sqrt{\bar{\bar{\eta}}^2}\tilde{\bar{\xi}}}{\sqrt{2}}, \frac{\bar{\bar{\eta}}-\sqrt{\bar{\bar{\eta}}^2}\tilde{\bar{\xi}}}{\sqrt{2}}\right)$
$\square$	① $1+\eta_s \neq 0$	$\left[\frac{\xi_s-1}{\eta_s+1}\frac{\bar{\bar{\eta}}}{\sqrt{\bar{\bar{\eta}}^2}}, \frac{\xi_s+1}{\eta_s+1}\frac{\bar{\bar{\eta}}}{\sqrt{\bar{\bar{\eta}}^2}}\right]$	$(0, \eta_s+1]$	$\left(-\sqrt{\bar{\bar{\eta}}^2}\tilde{\bar{\xi}}, -\bar{\bar{\eta}}\right)$
	② $1-\xi_s \neq 0$	$\left[\frac{\eta_s-1}{1-\xi_s}\frac{\bar{\bar{\eta}}}{\sqrt{\bar{\bar{\eta}}^2}}, \frac{\eta_s+1}{1-\xi_s}\frac{\bar{\bar{\eta}}}{\sqrt{\bar{\bar{\eta}}^2}}\right]$	$(0, 1-\xi_s]$	$\left(\bar{\bar{\eta}}, -\sqrt{\bar{\bar{\eta}}^2}\tilde{\bar{\xi}}\right)$
	③ $1-\eta_s \neq 0$	$\left[\frac{-1-\xi_s}{1-\eta_s}\frac{\bar{\bar{\eta}}}{\sqrt{\bar{\bar{\eta}}^2}}, \frac{1-\xi_s}{1-\eta_s}\frac{\bar{\bar{\eta}}}{\sqrt{\bar{\bar{\eta}}^2}}\right]$	$(0, 1-\eta_s]$	$\left(\sqrt{\bar{\bar{\eta}}^2}\tilde{\bar{\xi}}, \bar{\bar{\eta}}\right)$
	④ $1+\xi_s \neq 0$	$\left[\frac{-1-\eta_s}{1+\xi_s}\frac{\bar{\bar{\eta}}}{\sqrt{\bar{\bar{\eta}}^2}}, \frac{1-\eta_s}{1+\xi_s}\frac{\bar{\bar{\eta}}}{\sqrt{\bar{\bar{\eta}}^2}}\right]$	$(0, 1+\xi_s]$	$\left(-\bar{\bar{\eta}}, \sqrt{\bar{\bar{\eta}}^2}\tilde{\bar{\xi}}\right)$

References

[1] N. A. Dumont. On the efficient numerical evaluation of integrals with complex singularity poles. *Engineering Analysis with Boundary Elements*, vol. 13, pp. 155–168, 1994.

[2] N. A. Dumont and M. Noronha. A simple, accurate scheme for the numerical evaluation of integrals with complex singularity poles. *Computational Mechanics*, vol. 22, n. 1, pp. 42–49, 1998.

[3] N. A. Dumont. An assessment of the spectral properties of the matrix G used in the boundary element methods. *Computational Mechanics*, vol. 22, n. 1, pp. 32–41, 1998.

[4] N. A. Dumont. The collocation boundary element method revisited: Perfect code for 2D problems. *International Journal of Computational Methods and Experimental Measurements*, vol. 6, n. 6, pp. 965–975, 2018.

[5] N. A. Dumont. The consistent boundary element method for potential and elasticity: Part I — formulation and convergence theorem. *EABE - Engineering Analysis with Boundary Element Methods*, vol. 149, pp. 127–142, 2023a.

[6] N. A. Dumont. The consistent boundary element method for potential and elasticity: Part II — machine-precision numerical evaluations for 2D problems. *EABE - Engineering Analysis with Boundary Element Methods*, vol. 149, pp. 92–111, 2023b.

[7] N. A. Dumont. The consistent boundary element method for potential and elasticity: Part III — topologically challenging numerical assessments for 2D problems. *Engineering Analysis with Boundary Element Methods*, vol. 151, pp. 548–564, 2023c.

[8] N. A. Dumont. Complex-variable, high-precision formulation of the consistent boundary element method for 2D potential and elasticity problems. *Engineering Analysis with Boundary Element Methods*, vol. 152, pp. 552–574, 2023d.

[9] N. A. Dumont. Consistent boundary element method for two-dimensional problems of elasticity with geometry-preserving, homothetic element generation. *Journal of Elasticity*, vol. 157, n. 3, pp. 59–98, 2025.

[10] J. A. Cottrell, T. J. R. Hughes, and Y. Bazilevs. *Isogeometric Analysis: Toward Integration of CAD and FEA*. John Wiley and Sons, 2009.

[11] N. A. Dumont. Consistency, precision, and accuracy assessment of the collocation boundary element method for two-dimensional problems of potential and elasticity. *Archive of Applied Mechanics*, 2024.

[12] O. C. Zienkiewicz. *The Finite Element Method*. McGraw-Hill, 1977.

[13] D. A. Dunavant. High degree efficient symmetrical Gaussian quadrature rules for the triangle. *International Journal for Numerical Methods in Engineering*, vol. 21, pp. 1129–1148, 1985.